PAPER

Designing compliant mechanisms composed of shape memory alloy and actuated by induction heating

IOP Publishing Smart Materials and Structures
Smart Mater. Struct. **30** (2021) 095025 (11pp) https://doi.org/10.1088/1361-665X/ac1b15

Designing compliant mechanisms composed of shape memory alloy and actuated by induction heating

Adrien Thabuis[1], Sean Thomas[1], Thomas Martinez, Paolo Germano and Yves Perriard*

Integrated Actuators Laboratory (LAI), Swiss Federal Institute of Technology Lausanne (EPFL), Neuchâtel Branch, Switzerland

E-mail: yves.perriard@epfl.ch

Received 14 March 2021, revised 28 June 2021
Accepted for publication 5 August 2021
Published 18 August 2021

Abstract

Shape memory alloys (SMAs) are a type of smart materials that reacts mechanically to heat. Due to their complex behavior, they are often used in a simple geometry such as wires. This constrains the output displacement of the alloy to a simple linear contraction of the wire. When a different output displacement is desired, the SMA is coupled to a mechanism that transforms the motion, degrading the compactness of the whole system. To alleviate such issues, we propose fabricating, directly in SMA, a compliant mechanism that performs complex output motions and thus improves integration. The first part of this paper presents a method to design such systems. When coupled with a bias-spring and a heating system, these mechanisms form a full actuator. The conventional heating system relies on Joules losses coming from direct electric conduction through the alloy. However, now that the SMA has a complex shape, passing a current through it becomes an arduous task requiring multiple electrodes making the system cumbersome and deteriorating its integrability. Magnetic induction heating is proposed to tackle this limitation, heating the mechanism without contact and conserving a compact actuator.

Keywords: actuator, smart materials, bias-spring, topology optimization, coil

(Some figures may appear in colour only in the online journal)

1. Introduction

In the growing age of miniaturization, the need for compact and lightweight actuators has reached critical mass. Smart materials, which provide work when exposed to a certain stimulus, have become prime candidates to create integrated and compact actuators. A shape memory alloy (SMA) is a brand of smart materials that can be magnetically [1], or thermally activated. The NiTiNOL alloy, which is a type of thermally activated SMA, can be easily obtained in various shapes such as wires, springs, and sheets. It is shown to have higher energetic costs and lower fatigue life [2] but presents with the highest volumetric work density among the other smart materials [3]. This makes it the perfect candidate for the miniaturization of actuators [4], and will then be the one used for this research.

Generally, SMAs are shaped as simple wires or springs so as to more easily predict the behavior when the alloy is heated or cooled. The most common type of implementation of shape memory alloys into an actuator is bias-spring SMA actuators. They are simple linear actuators where the SMA component is paired with a passive spring. Here, the actuator performs a linear motion based on its temperature. One possible explanation for the prevalence of this type of 1-dimensional (1D) implementation could be due to the complex nature of these alloys and the difficulty to model and predict their behavior. But in certain contexts, these 1D structures can in fact be the best solution.

[1] These authors contributed equally to this work.
* Author to whom any correspondence should be addressed.

In practice, when complex motion is achieved by SMA actuators, there are either composed of multiple 1D SMA systems in series [5, 6], or coupled with a mechanism that transforms the linear motion into the desired one [6, 7]. This mechanism can be a cumbersome one composed of a multitude of pieces [8] or be a compliant one relying on elastic deformation [9, 10]. Some works have been conducted to creating SMA actuators using compliant SMA structures with positive results [11–13] but due to the complexity of the structure, designing such mechanisms is difficult.

Topology optimisation (TO) has been essential in designing transducer systems that can take simple inputs and elastically transform them into the required more complex outputs [14]. These compliant mechanisms designed by TO can be quite effective in creating compact solutions. Generally, they are used as a converter of motion but have also been known to be paired with smart materials such as piezoelectric ones [15]. Combining this design methodology with SMAs can be quite difficult due to the complex and non-linear nature of the alloy [16].

The goal of this paper is to provide a robust method to design integrated actuators composed of SMA, and exhibiting complex grasping capabilities. As the modeling of a shape memory alloy can be challenging, we propose a method that does abstraction of its multi-physics and non-linear properties while designing, but still accounts for the desired behavior of the smart material. This permits the algorithm to quickly design multiple smart actuators with high resolution and avoids the conventionally huge simulation time required when designing iteratively. The work presented in [17, 18], validates the methodology using finite element modeling (FEM), while in this paper, the methodology is further validated experimentally with a prototype showing the presence of the shape memory effect. Additionally, due to the complex nature of the proposed topologies, a novel heating solution is presented in this work, using magnetically induced current which allows for the actuation of such an actuator and further helps to validate the design methodology.

The paper is organized as follows: in section 2 the shape memory effect (SME) is presented as well as its integration into actuators; in section 3 the method to design the compliant mechanisms is presented and applied to some benchmark problems. In section 4, the presence of the SME is experimentally validated with a prototype. A novel heating method relying on magnetic induction is proposed and experimentally validated in section 5. Then, in section 6, the proposed methodology is applied to multi-output SMA actuators. Finally, the manufacturing perspectives of such actuators are discussed as well as the limitations and possible improvements of the proposed approach in section 7.

2. SMAs

2.1. SME

The physical effect observed in SMAs, commonly referred to as the SME, is a complex behavior dependant on multiple variables. In essence, the structure of such alloys, at low temperature, can be 'plastically' deformed and subsequently can be heated to a specific temperature to revert the deformation that it had undergone previously. This phenomenon exists due to various phase transformations that occur inside the alloy when it is subjected to stress and temperature. In figure 1, a simplified diagram shows the SME as the material transitions through its three states. At low temperature and low stress, the SMA exists in the twinned Martensite (M) phase. When a critical stress is applied, the alloy deforms and undergoes a process known as detwinning, where the internal structure changes, to convert to the detwinned M state. In this state, the material will retain the imposed strain even if the stress is released. When the structure is then heated to a specific temperature, known as the transformation temperature, the SMA will undergo the Austenite (A) phase transformation and the retained strain will be recovered, reverting the structure back to its initial shape. Finally, when the alloy is cooled down, it transforms back to the initial twinned M phase where the material can be once again deformed.

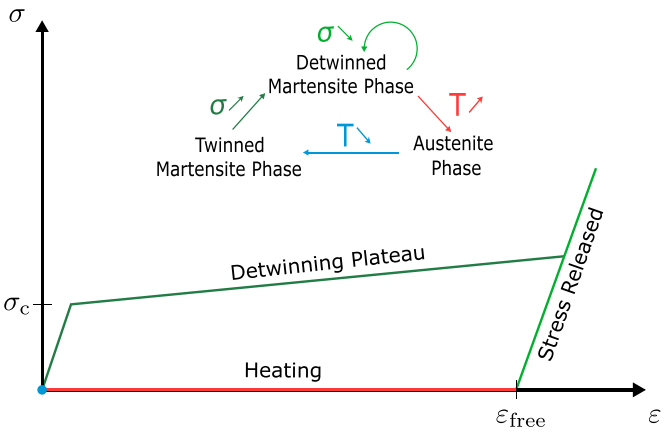

Figure 1. Stress–strain (σ-ε) curve of an SMA with associated state transformations.

It is understood that there is a requirement to pre-deform the SMA structure, so as to observe a strain recovery and thus work when heating. Therefore, it is commonly referred to as activating the material or active material when the SMA is detwinned. This critical stress, required to transform the material from the twinned M state to the detwinned M state, is the threshold for enabling the shape memory effect.

2.2. Bias-spring actuator

As previously mentioned, the critical stress is required to activate the material. This criterion can be achieved in numerous different ways, either using passive elements such as dead weights, springs, compliant mechanisms [19], or using an active element such as an antagonistic SMA [6]. The most common method to create an SMA-powered actuator is to attach the smart material to a passive bias-spring [20]. This allows the material to be activated by the spring as the material cools down and to elongate the spring as the material heats up, resulting in a cyclical linear actuation. In figure 2, a schematic of the working principle of a bias-spring SMA actuator can be

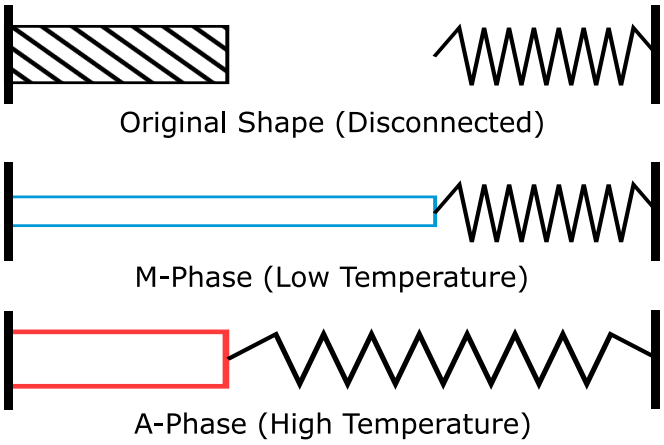

Figure 2. Principle of SMA bias-spring actuators.

seen. This simple system is quite effective due to its simplicity and compact footprint.

3. Design method of the compliant mechanism

We propose to realize the transducer that transforms a linear input motion into a complex output, under the form of a compliant mechanism directly made from the shape memory alloy. This will permit better integration capabilities as there are fewer pieces than the conventional approach where the transducer has to be connected in series with the smart alloy.

As detailed later in section 3.1, the design method couples an optimization problem with finite element analysis (FEA), which can result in large computational time if not carefully accounted for. Furthermore, for highly non-linear materials such as SMA, such analyses are not trivial to pursue as some convergence issues may arise in addition to the really large computational time. To achieve efficient computation and fast optimization, we propose to avoid the multi-physic and non-linear properties of the smart material while designing. Therefore, we consider compliant mechanisms made of a standard elastic material with linear properties and no thermal dependency. The distributed compliant nature of the resulting mechanisms make them ideal candidates to be actually fabricated in SMA. It is a crucial aspect of the proposed method as it results in a tremendous gain of computational time. It also provides better scalability of the approach if it had to be extended to 3D topology optimization problems [21]. To summarize, to achieve fast computation, we design a compliant mechanism made of a standard linear material that once fabricated with the smart one, will exhibit adequate performances as an active actuator due to the shape memory effect.

3.1. Topology optimization of the compliant mechanism

The most famous numerical method to design compliant mechanisms is the TO one which formulates the design problem as an optimization one. It relies on FEA to evaluate the behavior of the design according to physical laws. This method directly investigates the distribution of material inside a design

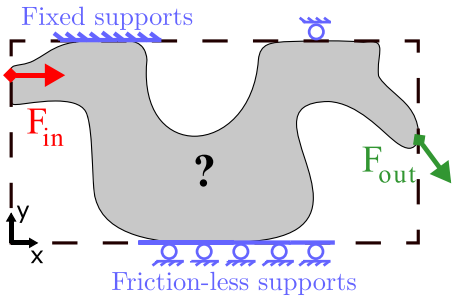

Figure 3. General problem for the design of a compliant mechanism.

space, providing a huge amount of freedom in the achievable topologies. These attractive features have made the TO method a large subject of research in recent years [22]. The so-called density-based approach for TO was chosen for this research because it is the most straightforward to implement, with great robustness and efficient computation time [23].

The initial goal is to determine the correct distribution of material into the design space, that generates the desired output displacement under a specific input load (as shown in figure 3). Topology optimization is performed on a design space discretized into nodes and cells/elements forming a mesh. The design variables are artificial densities ρ_e representing the amount of material that fills each element e. Each variable varies from a minimal value close to 0, to 1. The lower and upper bounds correspond to *full*-materials: air and solid respectively. The other values contained between these two bounds are defined as *intermediate*-materials. They correspond to a mathematical mean to extend the initial discrete material description (air or solid) to a continuous one (from air to solid). This permits the use of gradient-based optimization and avoids integer programming which is not computationally efficient for such large problems [24]. *Intermediate*-materials are not desired in the final topology to have a manufacturable solution and thus, are penalized during the optimization. This is performed while mapping the design variables to their corresponding material properties, here the Young modulus E, under the form of a Material Interpolation Scheme (MIS). Numerous schemes exist [23] but we chose to implement the SIMP one:

$$\mathrm{E}_e = \mathrm{MIS}(\rho_e) = (\overline{\mathrm{E}} - \underline{\mathrm{E}})\rho_e^n + \underline{\mathrm{E}}, \tag{1}$$

with $\underline{\mathrm{E}}$, $\overline{\mathrm{E}}$ corresponding to the Young modulus of an 'empty' element (air) and one completely filled of material respectively. The actual values of these physical quantities are set to $1e^{-3}$ and 1000 respectively to prevent numerical instabilities [25]. The penalty factor n is continuously increased throughout the optimization to regulate the optimization problem and avoid a hasty convergence to a local optimum.

Two separate loading-cases are studied in order to properly evaluate the performances of the compliant mechanism. In the first one, a known actuation force $\mathbf{F_{in}}$ is applied at the input port, resulting in nodal displacements $\mathbf{U_{in}}$. A second loading-case is required to account for the effect of the reaction force of the workpiece [26]. Thus, a unit external load $\mathbf{F_{out}}$ is applied at the output port, resulting in nodal displacements $\mathbf{U_{out}}$. The two

different displacements correspond to the state variables of the optimization problem and are computed during an FEA. Small displacements are assumed but still provide a great approximation of how the mechanism behaves. In the end, the FEA is reduced to solving a simple matrix equality for each loading case: $\mathbf{KU_{in}} = \mathbf{F_{in}}$ and $\mathbf{KU_{out}} = \mathbf{F_{out}}$, with $\mathbf{K} = \mathbf{K}(\mathbf{E})$ the global *stiffness* matrix of the finite element space, which is built using the previously computed material properties [27]. These equations are not equality constraints enforced within the optimization problem, but are simply solved to determine the state variables used to compute the objective function.

The goal of the optimization is not limited to the design of a compliant mechanism that can achieve the desired motion transformation, but also targets distributing the strain over the whole mechanism. As further explained in section 3.2, this enables a maximal amount of activated material when the transducer will be fabricated in SMA. This goal is formulated as an objective function, which needs to be a scalar. It means that a global measure of the distributed strain is needed. The mutual strain energy S_{mut} between the input and output load is chosen because it still accounts for the desired motion transformation. As proposed in [26] the strain energy is divided by the sum of the input S_{in} and output S_{out} strain energies, to have a unitless and dimensionless objective function:

$$\gamma = \frac{S_{mut}}{S_{in} + S_{out}} = \frac{2 \cdot \mathbf{U_{out}}^{T} \mathbf{K} \mathbf{U_{int}}}{\mathbf{U_{out}}^{T} \mathbf{K} \mathbf{U_{out}} + \mathbf{U_{in}}^{T} \mathbf{K} \mathbf{U_{in}}}. \tag{2}$$

This permits to be less dependent on the design's scale, the magnitude of the loads, and improves the convergence and robustness of the optimization problem. This objective can be extended to multi-input multi-output compliant mechanisms by using the weighted sum of the former ratio restricted to each input-output couple. Different weights can be chosen to favor certain motion transformation couples over others. For each new loading-case, an additional FEA has to be performed to evaluate the displacement resulting from the new load. Artificial springs are placed at the input and output ports to simulate the input work and the resistance coming from the workpiece, respectively, as commonly done for TO of compliant mechanisms [26]. The optimization minimizes the objective function, so a minus sign is added in front of it to perform a maximization. The design variables are subject to a volume limitation, formulated as an inequality constraint in order to improve convergence as generally done for TO [25]. The optimization problem is formulated as follows:

$$\begin{aligned}
\min_{\boldsymbol{\rho}} : \quad & -\gamma(\mathbf{U_{in}}, \mathbf{U_{out}}, \mathbf{E}) \\
\text{s.t.:} \quad & \mathrm{Vol}(\boldsymbol{\rho}) < \mathrm{Vol}^{*} \\
& 0 < \rho_{\min} \leqslant \rho \leqslant 1 \\
\text{with:} \quad & \mathbf{K}(\mathbf{E})\mathbf{U_{in}} = \mathbf{F_{in}} \quad \mathbf{K}(\mathbf{E})\mathbf{U_{out}} = \mathbf{F_{out}} \\
& \mathbf{E} = \mathrm{MIS}(\boldsymbol{\rho}) \\
& \mathrm{Vol} = \left(\sum_{e=1}^{\mathrm{NE}} \rho_e \cdot V_e \right) / \left(\sum_{e=1}^{\mathrm{NE}} V_e \right).
\end{aligned} \tag{3}$$

The gradient of the objective function with respect to the design variables is required to update the design variables at each iteration. The adjoint variable method is used for this purpose because it is the most efficient method when the number of design variables is significantly larger than the number of functions to evaluate [28]. The solver is updating the design variables based on the objective function value and its gradient. In this work, the optimality criteria (OC) [25] and the method of moving asymptotes (MMA) [29] are implemented and used for the benchmark and actuator problems respectively. This choice was motivated by numerous works using these solvers for the design of compliant mechanisms [26]. After the update of the design variables, the process is performed again and repeated until a stopping criterion is reached. This could correspond to a maximum number of iterations or to the convergence of the objective function contained below a small value. The developed implementation is built upon [27], a published academic Matlab code for structural topology optimization.

3.2. Compliant mechanism made of SMA

The generated compliant mechanisms are great candidates to form efficient SMA-actuators. Indeed, for a compliant mechanism fabricated in SMA, it is desired to have the maximal volume of the material that undergoes detwinning, that is being activated to fully harvest the SME of the smart alloy. This is ensured by distributing the strain over the whole mechanism while transforming the motion, which prevents having regions that do not reach the critical stress activating the material. The distribution of strain is enforced by the chosen objective function that maximizes the mutual strain energy. This maximizes the amount of deformed areas within the mechanism, reducing the quantity of passive regions within the structure.

3.3. Simulation results of benchmarks problems

The proposed method is applied to three benchmark problems to be validated: an inverter, a crimper, and a gripper. All of them are fixed at their bottom and top left corners (corresponding to ideal pivots), but differ by the position of the input and output forces. The design problems and the resulting topologies are shown in figure 4. The artificial springs are only necessary while optimizing and are thus removed from the resulting mechanisms. The optimizations are performed on half the design domain due to the symmetry of the problems. Frictionless supports are imposed on the symmetry axis to account for it in the analysis. This half-domain is discretized into 10 000 elements. The design variables are all initialized uniformly so as to satisfy the volume fraction constraint of 30%. The stiffness of the artificial springs is set to 0.1, and the input forces to 1. The optimizations are run on a Windows workstation with an Intel i7 3.6 GHz, 8-core processor, and 32G memory. The complete process takes less than a minute to converge for each of the benchmark problems. One can note, that the computation time is really short and would have been of a significantly larger order of magnitude if non-linear and multi-physic analyses were performed.

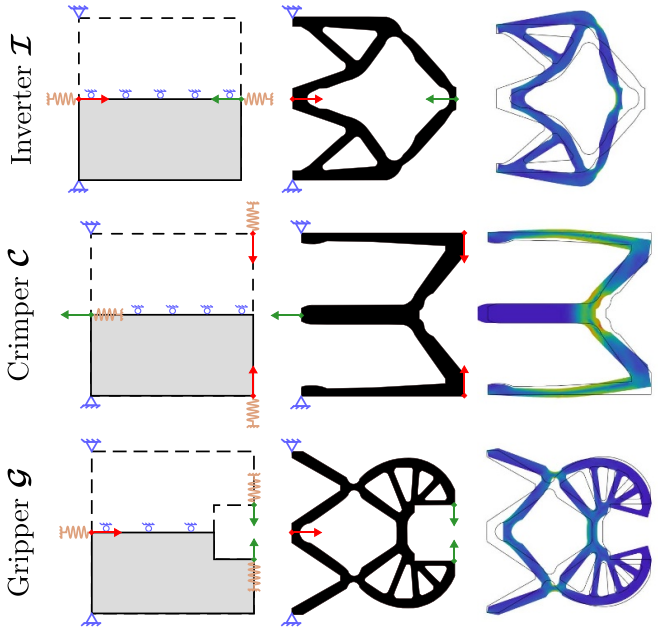

Figure 4. Generated benchmark compliant mechanisms with normalized stress distribution in the deformed state. The input forces are shown in red and the output forces in green.

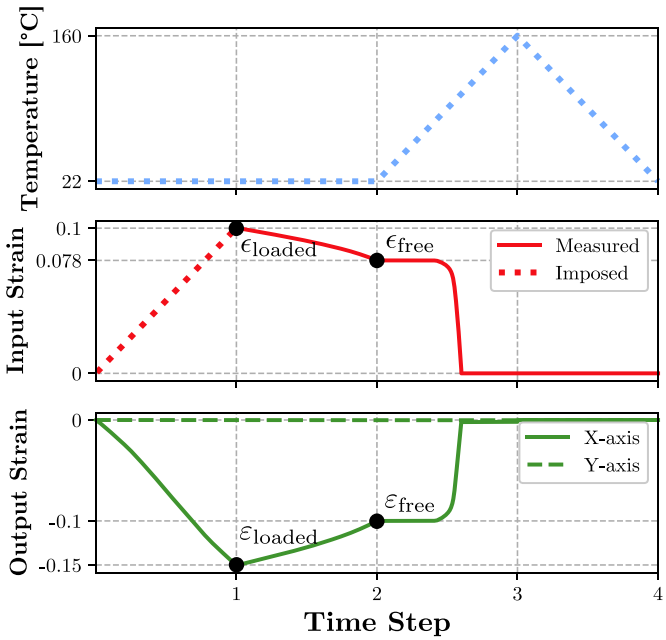

Figure 5. Simulation of the SMA-inverter validating the shape memory effect. This topology presents a strain retention of 77.6%.

Table 1. Results of the SME for the benchmark problems: $\mathcal{I}$ Inverter, $\mathcal{C}$ Crimper, $\mathcal{G}$ Gripper.

	$\epsilon^x_{\text{loaded}}$	$\epsilon^y_{\text{loaded}}$	ϵ^x_{free}	ϵ^y_{free}	α^x_ϵ	α^y_ϵ
$\mathcal{I}$	0.149	—	0.103	—	**77.6%**	—
$\mathcal{C}$	−0.061	—	−0.048	—	—	**75.2%**
$\mathcal{G}$	0.015	−0.085	0	−0.065	**77.6%**	—

In order to validate the presence of the shape memory effect, characterized as an ability to retain its deformed shape, a multi-physics (structural and thermal) and non-linear FEA of the resulting designs is performed on ANSYS. The four different simulated steps are illustrated in figure 5 using the inverter design but have been similarly done for the other problems. An input displacement is first applied, generating a displacement at the output, $\varepsilon_{\text{loaded}}$. If every deformed area has undergone the detwinning process, the structure should keep the deformed shape when the input displacement is released after the first time step, excluding a slight elastic spring back of the material. However, as some parts of the compliant mechanism are not sufficiently strained, the degree of detwinning within the structure is not uniform and a portion of the strain will be lost when the input displacement is released. Thus, the observed strain at the output will decrease to $\varepsilon_{\text{free}}$. During the third time step, the structure is heated to be reverted back to its original shape and all the strain is recovered. Finally, the structure is cooled down to return the material to its initial phase. The normalized stress distributions associated with the deformed mechanisms at the first time step are shown on the right-hand side of figure 4.

There is a need for a measure by which the results can be compared. The final goal being to integrate these SMA-compliant mechanisms into bias-spring actuators, the measure should represent how well the work stored by the biasing element is converted to a useful one capable of detwinning the SMA. This could be formulated as a measure of the relative quantity of material activated (detwinned) by the biasing element. The larger this quantity is, the more optimal the actuator will be. The amount of detwinned material can be roughly estimated using the principle that it behaves as a plastically deformed one. In other words, it is the quantity of material that retains its shape after the deformation load is removed. This factor is expressed in equation (4) as the strain retention factor. It is defined as the amount of strain observed in the structure after the deformation load is released. This factor will vary between a value of 0 implying no activated material and no strain retention, and a value of 1 for a perfectly detwinned material with the entirety of the strain retained when the load is released. It is calculated as:

$$\alpha_\epsilon = 1 - \frac{\epsilon_{\text{loaded}} - \epsilon_{\text{free}}}{\epsilon_{\text{loaded}}}, \tag{4}$$

with ϵ_{loaded} and ϵ_{free} representing the domain space normalised input displacement at time steps 1 and 2 respectively. Due to the fact that even at high stresses, the detwinned (M phase) SMA is not infinitely rigid and results in elastic behavior as seen in figure 1, a perfectly detwinned material will not achieve a perfect strain retention of 1. Nevertheless, for a given input deformation, the strain retention factor can be used to qualitatively compare the ability of the structure to show the shape memory effect when heated. Therefore, it provides an effective way to compare the different benchmark problems and multi-output actuator designs based on their capacity to function as an SMA actuator. The results from table 1 show that the strain retention factor is quite high for all the designed mechanisms. By showing that, as 75% of the strain

being retained when the applied load is released, the structure will recover most of its deformation when heated. One can, thus, conclude that realizing a compliant mechanism in SMA with maximal mutual strain energy, will result in a structure with a large strain retention factor. This implies that the algorithm, without explicitly considering the material properties of the SMA, can create a compliant mechanism that will effectively show the shape memory effect. This presents an attractive solution for developing compliant mechanisms made entirely of SMA while still being able to exploit its SME.

4. Experimental validation of the strain retention

The goal of this section is to validate experimentally the proposed design approach. Therefore, a prototype of an SMA compliant mechanism is realized and mounted on a pull-tester to measure its strain retention factor and compare it to the simulated one. The fabricated prototype is mounted to the pull-tester, as shown in figure 6 and the force-displacement of the structure is measured.

The inverter is chosen to realize the prototype because its input and output ports are preferred to be mounted on a pull-tester. The benchmark problem assumes clamped single nodes, which corresponds to ideal pivots as boundary conditions. It is not a realistic choice for the realization of a test-bench. Multiple nodes are thus clamped on the left side covering a tenth of the design domain height from each corner. This results in a slightly modified inverter structure as seen in figure 6. Furthermore, the modified inverter structure is simulated in FEM, similarly to the benchmark problems, so as to compare the same topology present in the experimental prototype. The stress distribution across the mechanism is similar to the benchmark version of the inverter displayed in figure 4. The parts with higher strain could be targeted as regions to heat in order to actuate the mechanism.

Regarding the manufacturing of such a mechanism, a monolithic block of NiTiNOL could be machined. However, this would incur a high cost and lead to a large amount of wasted material so this solution is discarded. The topology being 2-Dimensional (2D), it is fabricated by laser cutting a thin sheet of NiTiNOL (55.8 wt. % Ni) purchased from *Memry Corporation*. Some supporting plates in PMMA sandwich the smart material to minimize its buckling along the third dimension while assuring the same 2D deformation. The advantages of this method of fabrication, to test the validity of the design methodology, include the reduced cost of the prototype and more importantly, assure that the stress and strain distribution of the 2D sheet will be similar to a 3D structure with the same form. This means that the output displacement will be similar to the intended 3D structure. The disadvantage of this PMMA sandwiched prototype is the added friction to the structure. This implies that the pull-tester will require more force to strain the structure. In summary, if the PMMA plates tightly compress the SMA structure, this will result in a more accurate output displacement by preventing unwanted buckling but increase the force requirement. Thus, a trade-off is

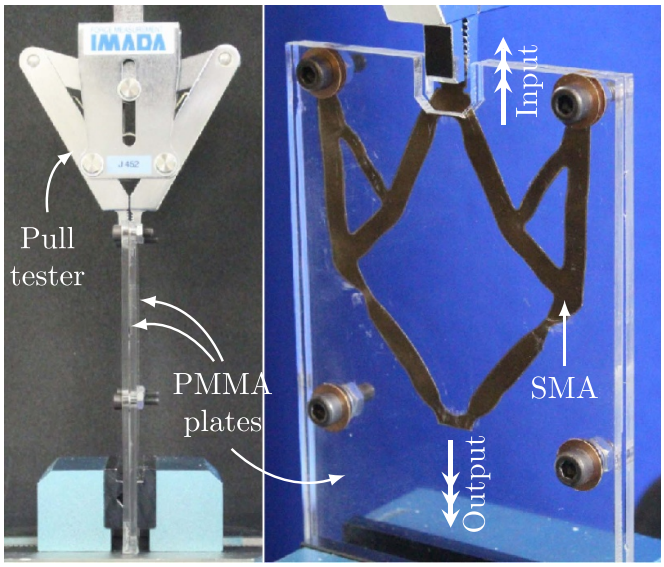

Figure 6. The experimental setup of the inverter prototype. The prototype is cut from a thin SMA sheet and is sandwiched between PMMA sheets to prevent buckling. The input load is applied using the pull-tester while measuring the input displacement and force. The output displacement is recorded using a microscopic camera.

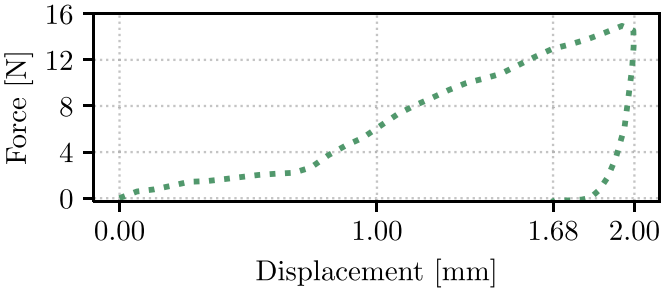

Figure 7. The experimental results of the inverter prototype are obtained using a pull-tester and a strain retention of 84.3% is observed.

Table 2. Comparison between the FEM and experimental results of the modified inverter benchmark problem.

	x_{loaded} (mm)	x_{free} (mm)	α_ε (%)
FEM	2.0	1.58	78.9
Expt	2.0	1.68	84.3

present but due to the strain retention factor, as described in (4), requires only the input displacement, the prototype was fabricated to prioritize the fidelity of the input strain. Thus, when comparing the pull-tester results with the FEM simulation, only the input displacement should be compared and not the force requirements.

In figure 7, the pull-tester results can be observed. Here the strain retention is measured by applying the initial strain to the prototype and then reversing the direction of the pull-tester while measuring the reaction force. The retained strain is measured at the point in which the measured force descends

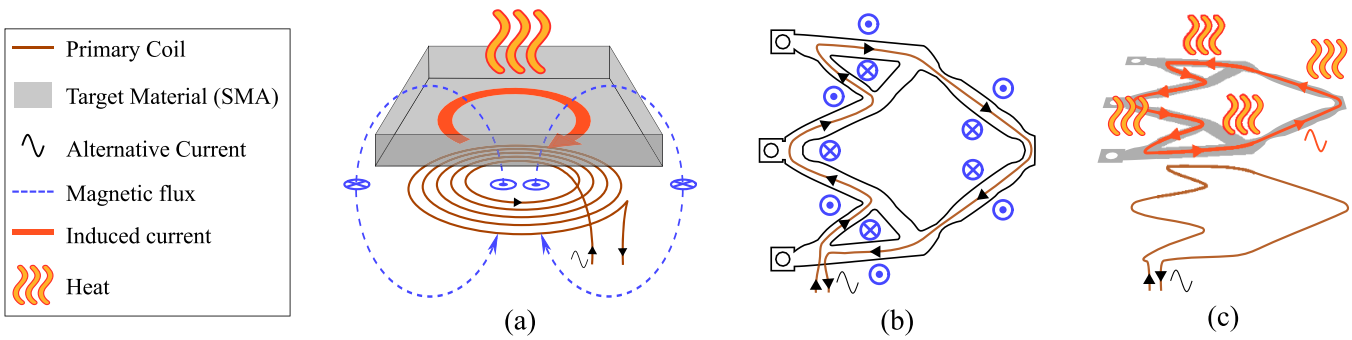

Figure 8. Induction heating—(a) general principle, (b) 2D view of the coil designed for the deformed inverter, with the direction of the generated magnetic flux normal to the plane, (c) 3D view of the induction system for the inverter problem.

below 0N and the prototype starts to bend on itself. When the pull-tester observes a value below −0.2N, this implies the structure has overcome the internal friction and the pull-tester is now bending the prototype instead. Based on these values, a strain retention of 84.3% is observed. When compared to the strain retention of 78.9% in the conducted FEM simulation of the same modified inverter topology, it shows that the FEM simulations can be validated. The results are summarized in table 2. This difference in the strain retention is explained by the increased friction present between the thin SMA sheet and the PMMA plates. Furthermore, when the structure is heated, the strain is completely recovered and the structure reverts back to its original shape. These results validate the fact that the shape memory effect can indeed be observed from these topologies.

5. Proposed heating method

A heating system is required to control the whole actuator. As SMAs are relatively good electrical conductors [30], direct Joules heating of the SMA is often preferred as heat is directly generated from inside the material, permitting a simpler solution and a more integrated actuator. The element to heat, being usually a simple wire, is actuated by simply attaching electrodes to its extremities and passing the electric current. However, if the SMA has a complex shape, as proposed in this research, passing the correct current becomes quite a substantial task. Indeed, as the paths of the current are not unique nor trivial anymore, multiple electrodes are necessary, requiring multiple external wires to be connected to the moving structure. This deteriorates the size of the actuator as well as the robustness of the whole system. While an external heater coil can be attached to the surface of the actuator as presented in [31, 32], this can prove to be quite difficult to implement due to the possible delamination of the external coils as the SMA element deforms. Furthermore, adding a bonding material can reduce the thermal exchange properties. In this work, it is proposed to induce magnetically the current inside the alloy, removing the need to attach anything to the moving SMA. This method permits to heat the structure without any physical contact and requires only one coil instead of multiple electrodes with many wires.

5.1. Magnetic induction heating

The principle of magnetic induction heating and its application to the inverter mechanism are shown in figure 8. A current alternating at generally high frequency is passed through a primary coil, which generates an alternating magnetic field. When an electric conductor is placed inside this varying field, a secondary electric current I_{induced} is induced inside the piece. This current creates Joules losses P_{Joules} heating the piece:

$$P_{\text{Joules}} = R_{\text{SMA}} \cdot I_{\text{induced}}^2 = \frac{V_{\text{emf}}^2}{R_{\text{SMA}}}. \tag{5}$$

The induced current depends on the electromotive force V_{emf} generated by the primary coil, and the effective resistance R_{SMA} of the path taken by the induced current. The electromotive force depends on the coupling between the primary coil and the SMA part to heat:

$$V_{\text{emf}}^2 = \left(-\frac{\mathrm{d}\Psi}{\mathrm{d}t}\right)^2 = \left(-2\pi f L \cdot I_{\text{prim}}\right)^2 \tag{6}$$

with Ψ the total flux linkage between the primary and SMA side, f the working frequency, I_{prim} the RMS value of the primary current and L the mutual inductance between the primary coil and the SMA.

The input current I_{prim} is maximized for a minimal resistance of the primary coil because a voltage source is used to power the system. It is further increased by connecting the coil to a capacitor, creating a resonating circuit. As shown in (6), a large working frequency is desired for maximal induced heating. However, at high frequencies, undesirable effects arise such as skin and proximity effect increasing the resistance of the primary coil. Additionally, the parasitic capacitor of the impedance of the coil will also take-over above a critical frequency, canceling its inductive effect. The working frequency is thus limited, and is chosen to balance the losses on the primary side while still providing a large current at the resonant value. The mutual inductance between the coil at the primary side and the SMA at the secondary side is maximized for a large covered area and a large number of turns. The area being constrained by the shape of the alloy, it cannot be increased too much. Regarding the number of turns of the coil, it is limited by the associated increase of resistance which reduces the input current magnitude. One can observe

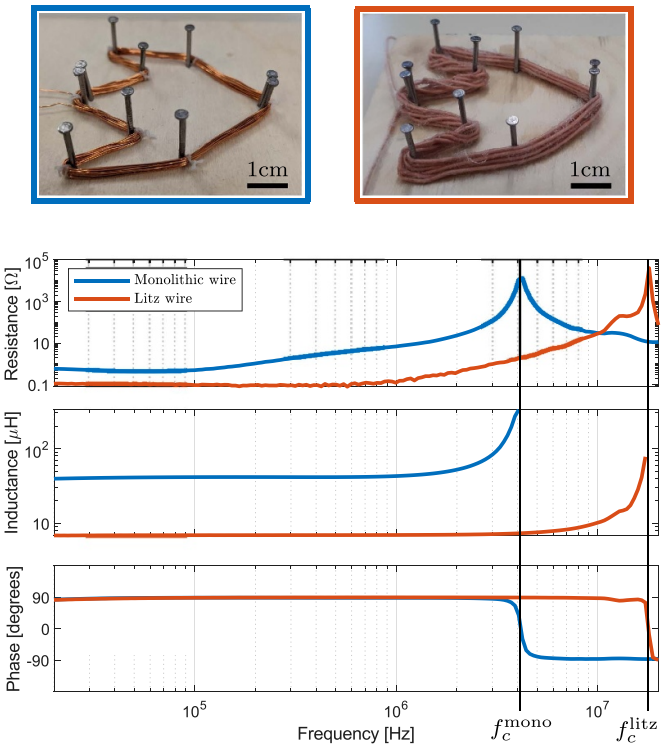

Figure 9. Comparison of primary coil with different types of wire. As the impedance becomes mainly capacitive over its critical frequency, the inductance's values after $f_c^{\text{mono}} = 17$ MHz and $f_c^{\text{litz}} = 41$ MHz are removed for the monolithic and Litz wire respectively.

that, as with many engineering problems, the sizing of the coil results in a complex trade-off that is case-dependent.

5.2. Design and experiments

The shape of the coil is determined to induce the current through the deformed parts of the SMA compliant mechanism. Some nails are placed inside a wooden plate to help to maintain the desired shape while winding. Once realized, a varnish is distributed over the coil to fix the shape and maintain the turns together after the nails are removed. Two prototypes are presented here: one with 25 turns of a standard monolithic wire with a copper diameter of 0.30 mm, and another composed of 15 turns of a Litz wire composed of 300 strands with a diameter of 0.040 mm each. Fewer turns were made for the second coil as the Litz wire is less compact and the total thickness of the coil should not be too large. As shown in figure 9, the wire's resistance increases significantly with the frequency due to the skin and proximity effect. Thus, a wire with a thinner effective cross-section, like the Litz wire, is preferred as this effect is reduced. The choice of the working frequency is crucial for the heating system. As shown in equation (6), it should be as high as possible for maximal Joules heating. However, it is limited by the parasitic capacitor of the coil, which *takes-over* the impedance above a critical frequency: $f_c^{\text{mono}} = 17$ MHz and $f_c^{\text{litz}} = 41$ MHz for the coil made of monolithic and Litz wire respectively. Despite the lower inductance of the Litz coil,

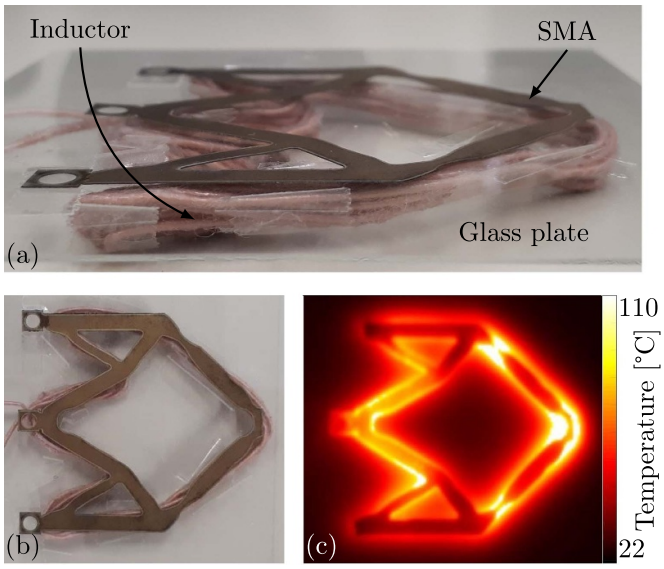

Figure 10. Induction heating system.

larger induction heating can be achieved because the working frequency and primary current can be much higher than the one with monolithic wire. Thus the coil composed of Litz wire is chosen for the heating system.

Based on the previous observations, it is decided to work around 4 MHz to have a large frequency but assure to be far enough from the critical one. At this frequency, the inductance of the coil is $L = 7.4$ μH and its resistance $R = 0.4\Omega$. A high voltage capacitor of $C = 230$pF is placed in series with the coil to create a L-C circuit resonating at $f = (2\pi\sqrt{LC})^{-1} =$ 3.86MHz. The input source is realized with a half-bridge inverter composed of GaN transistors (EPC9024). A primary current of $I = 1.5$A is generated at the working frequency, dissipating 0.9W on the primary side. The associated increase of temperature of the coil is not significant, which permits a stable operation. If the coil was made of monolithic wire, it would have heated much more, resulting in a change of the resistance and inductance value preventing a stable operating point. Figure 10 illustrates the heating system of the prototype as well as the temperature distribution over the SMA. This image has been taken with a thermal camera FLUKE Ti25. A glass plate is placed between the primary and secondary sides to assure that the SMA is not heated by convection from the coil's heat. A temperature up to more than 120 °C is attained, validating the induction system as a heating method for the multi-output SMA compliant actuators. As the cross-section of the mechanism is not constant, the induced current density and thus the heat is not uniformly distributed among the structure. As further discussed in the next section, this could lead to some misalignment problems between the SMA and the inductor.

For this prototype, the penetration depth does not limit the excitation frequency as the piece to heat is really thin. Indeed, for 10 MHz, the penetration depth is still larger than the SMA sheet's thickness of 100 μm. However, if one wants to extend the proposed approach to thicker SMA parts, the penetration depth would be an additional parameter to account for when choosing the input frequency.

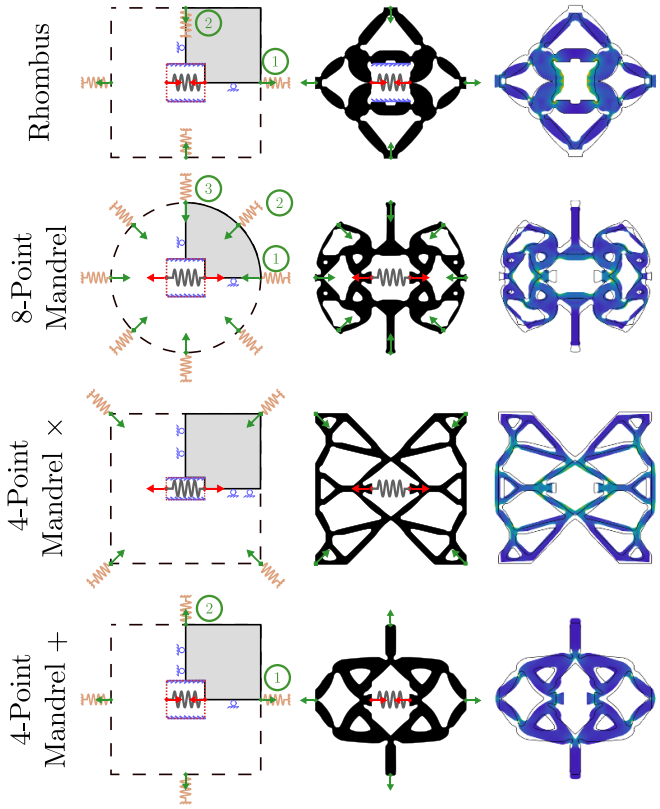

Figure 11. Generated multi-output SMA actuators with normalized stress distribution in the deformed state. The input forces are shown in red and the output forces in green. The artificial springs for TO are shown in brown while the bias-springs of the actuators are shown in grey.

6. Multi-output SMA actuators

The designed methodology, now validated using a benchmark problem and an experimental prototype, along with the proposed heating method, can be applied to create more complex structures that show the shape memory effect.

6.1. Generated multi-output compliant mechanisms

Various new multi-output actuators are proposed, with the SMA-compliant mechanism designed by the topology optimization method presented in section 3. They are shown in figure 11. The *rhombus* model is a multi-directional mechanism whose axes have opposing motions. It elongates in the y-axis and contracts in the x-axis. The other ones perform the task of an outer-mandrel in different ways: the 8-*point mandrel*, the 4-*point mandrel* $\times$ and the 4-*point mandrel* $+$. The evolution of the topology throughout the optimization for the 4-*point mandrel* $\times$ is given in figure 12. Just like the benchmark problems, the topologies, here, are generated while making abstraction of the shape memory effect and the nonlinear nature of the alloy. This greatly decreased the computational time required to generate these mechanisms as the whole optimization took less than two minutes for each one of them.

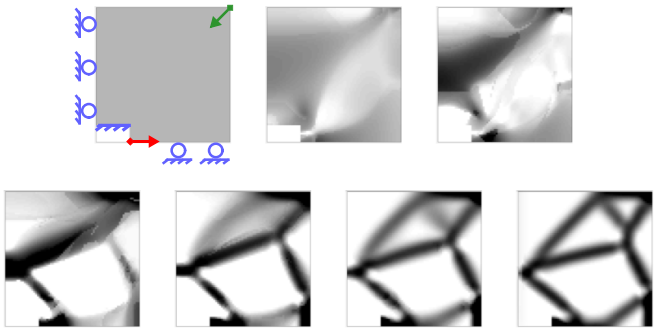

Figure 12. 4-point Mandrel $\times$: evolution throughout the optimization. The grayscale represents the value of the filtered artificial density. The input force is shown in red and the output force in green.

Following the same principle as the simulations presented in section 3.3, one can observe that the generated topologies exhibit the shape memory effect. An input strain of 10% is applied to each one of them at the center, where the bias spring is ideally attached, so as to have comparable results for each design. The results are summarized in table 3. The strain retention obtained for the generated actuators shows that a majority of the strain applied is retained and that heating the material will result in a considerable amount of actuation. These generated topologies show that the methodology is a viable solution for creating bias-spring SMA actuators.

6.2. Biasing-element

As shown in figure 11, the compliant mechanisms can be coupled with either a compression or a traction spring as a biasing element. This depends on the resting cooled position of the mechanism required by the application to which the actuator is integrated. The performed simulations are done assuming linear behavior of the material, which means that the type of spring used would not affect the resulting topology, only that the output displacement direction will be reversed. The resulting compliant mechanisms are relatively stiff. This is explained by the strain distributed over the whole structure which assures a maximal amount of detwinned SMA. This implies that a strong biasing element is required. Conventional spiral springs are too cumbersome for such stiffness. We propose to use a leaf-spring element that permits high stiffness in a compact space. For the proposed system, the leaf spring simply consists of an axially compressed flat sheet that has buckled. It can be sized to fit into the compact space within the topology. The rigidity of such a spring can be calculated based on the solution for the classic Euler beam problem as elaborated in [33].

7. Discussions

As the design method and the physics are the same between the model validated experimentally and all the actuators proposed in this paper, similar results are expected with all the transducers. They have not been realized here for convenience

Table 3. Results of the SME for multi-output actuators.

	$\epsilon^x_{\text{loaded}}$	$\epsilon^y_{\text{loaded}}$	ϵ^x_{free}	ϵ^y_{free}	α^x_ϵ
Rhombus	① : 0.051	① : 0	① : 0.042	① : 0	**67.9%**
	② : 0	② : 0.062	② : 0	② : 0.045	
8-Point Mandrel	① : −0.057	① : 0	① : 0.037	① : 0	**74.7%**
	② : −0.057	② : −0.05	② : −0.038	② : −0.034	
	③ : 0	③ : −0.085	③ : 0	③ : −0.058	
4-Point Mandrel ×	−0.029	−0.022	−0.023	−0.017	**81.4%**
4-Point Mandrel +	① : 0.051	① : 0	① : 0.042	① : 0	**68%**
	② : 0	② : 0.062	② : 0	② : 0.045	

and cost reasons. Indeed, SMAs are expensive materials so the best way to manufacture such complex structures would be with additive methods that avoid waste of material present for subtractive methods such as machining [34, 35]. Following the development over the last decade of such processes for various types of materials ranging from polymers to metals and alloys [36, 37], it is expected to happen for smart materials as well. Indeed some recent works have been published regarding the additive manufacturing of SMAs [38, 39]. With this method, multiple prototypes could be realized with fewer concerns about saving material. The proposed design approach will be a great tool to create novel smart actuators realizing complex motion.

Shape memory alloys are non-linear materials. Here, for the sake of computational time, the algorithm makes use of linear assumptions. This allows the domain space to be discretized to an even smaller scale and creates structures with higher resolution. The main drawback to this approach can be seen in the table 3 with the 8-Point Mandrel. Here the design was optimized to have the second output displacement occur at an angle of 45°. But the non-linear FEM shows that there is an error of 10% concerning the aforementioned output angle. By switching to a non-linear analysis for non-elastic deformation inside the optimization, the actual behavior could be better predicted but would significantly increase the computational time.

Furthermore, the induction system could be further improved through a better coil design. An algorithmic method, similar to the one proposed to design the compliant mechanism could be developed. As briefly introduced, misalignment from the moving compliant mechanism and the coil may happen. Indeed, as narrow SMA parts have larger resistance than others, they will heat more and reach the transition temperature earlier. These parts will then start regaining their initial shape sooner than the others. Depending on the configuration, this may cause the structure to be misaligned with the coil, compromising correct induction heating. This phenomenon hasn't been observed for the developed prototype.

8. Conclusion

This work presents a methodology to design bias-spring SMA actuators that are capable of complex outputs. The presented algorithm makes abstraction of the SME and the nonlinear nature of the alloy to create topologies that still show the shape memory effect while having a reduced computational time. Furthermore, a measure using strain retention is formulated to compare the different benchmark problems and the generated SMA structures. Using finite element analysis, the shape memory effect is observed and compared for the various topologies so as to validate the generative algorithm. The proposed method is robust and efficient, providing a great tool for engineers and researchers desiring to design such actuators.

An experimental prototype is fabricated using the shape memory alloy to validate the design approach and show that the SME is indeed observed after applying a thermal load. The heating of the prototype proved to be difficult using traditional Joules heating due to its complicated geometry. This work also presents a system in which the generated topologies can be heated using magnetic induction heating. Using the proposed heating solution and electronic circuit, the prototype was heated at a high enough temperature to exhibit the shape memory effect of the smart mechanism.

Data availability statement

All data that support the findings of this study are included within the article (and any supplementary files).

ORCID iDs

Adrien Thabuis https://orcid.org/0000-0001-6129-5971
Sean Thomas https://orcid.org/0000-0001-8705-9299
Thomas Martinez https://orcid.org/0000-0001-6366-1488

References

[1] Şaşmaz M, Bayri A and Aydoğdu Y 2011 The magnetic behavior and physical characterization of Cu–Mn–Al ferromagnetic shape memory alloy *J. Supercond. Nov. Magn.* **24** 757–62
[2] Fumagalli L, Butera F and Coda A 2009 SmartFlex NiTi wires for shape memory actuators *J. Mater. Eng. Perform.* **18** 691–5
[3] Mohd Jani J, Leary M, Subic A and Gibson M A 2014 A review of shape memory alloy research, applications and opportunities *Mater. Des.* **56** 1078–113
[4] Nespoli A, Besseghini S, Pittaccio S, Villa E and Viscuso S 2010 The high potential of shape memory alloys in developing miniature mechanical devices: a review on shape memory alloy mini-actuators *Sens. Actuators* A **158** 149–60

[5] Taylor A J, Slutzky T, Feuerman L, Ren H, Tokuda J, Nilsson K and Tse Z T H 2019 Mr-conditional SMA-based origami joint *IEEE/ASME Trans. Mechatronics* **24** 883–8

[6] Abubakar R A, Wang F and Wang L 2020 A review on NiTiNOL shape memory alloy heat engines *Smart Mater. Struct.* **30** 013001

[7] Furuya Y and Shimada H 1991 Shape memory actuators for robotic applications *Mater. Des.* **12** 21–8

[8] Singh P and Ananthasuresh G K 2013 A compact and compliant external pipe-crawling robot *IEEE Trans. Robot.* **29** 251–60

[9] Hwang D and Higuchi T 2016 A planar wobble motor with a xy compliant mechanism driven by shape memory alloy *IEEE/ASME Trans. Mechatronics* **21** 302–15

[10] Yao T, Wang Y, Zhu B, Wei D, Yang Y and Han X 2020 4d printing and collaborative design of highly flexible shape memory alloy structures: a case study for a metallic robot prototype *Smart Mater. Struct.* **30** 015018

[11] Kohl M, Just E, Pfleging W and Miyazaki S 2000 SMA microgripper with integrated antagonism *Sens. Actuators* A **83** 208–13

[12] Torres-Jara E, Gilpin K, Karges J, Wood R and Rus D 2010 Compliant modular shape memory alloy actuators *IEEE Robot. Autom. Mag.* 17 78–87

[13] Koledov V, Shavrov V, Fawzy M, Blumenthal M, von Gratowski S, Irzhak A, Shelyakov A and Topic M 2015 Nano-nanomanipulation of CdSe nanowires using nano-tweezers based on shape memory alloys *2015 Int. Conf. on Manipulation, Manufacturing and Measurement on the Nanoscale (3M-NANO)* pp 69–73

[14] Liu C-H, Chung F-M, Chen Y, Chiu C-H and Chen T-L 2020 Optimal design of a motor-driven three-finger soft robotic gripper *IEEE/ASME Trans. Mechatronics* **25** 1830–40

[15] Ruiz D and Sigmund O 2018 Optimal design of robust piezoelectric microgrippers undergoing large displacements *Struct. Multidiscip. Optim.* **57** 71–82

[16] Langelaar M, Yoon G H, Kim Y Y and van Keulen F 2011 Topology optimization of planar shape memory alloy thermal actuators using element connectivity parameterization *Int. J. Numer. Methods Eng.* **88** 817–40

[17] Thabuis A, Thomas S, Martinez T and Perriard Y 2020 Shape memory effect of benchmark compliant mechanisms designed with topology optimization *2020 IEEE/ASME Int. Conf. on Advanced Intelligent Mechatronics (AIM)* pp 571–6

[18] Thomas S, Thabuis A, Martinez T and Perriard Y 2020 Multi-output compliant shape memory alloy bias-spring actuators *2020 IEEE/ASME Int. Conf. on Advanced Intelligent Mechatronics (AIM)* pp 795–800

[19] Airoldi A, Rigamonti D, Sala G, Bettini P, Villa E and Nespoli A 2021 Development of an actuated corrugated laminate for morphing structures *Aeronaut. J.* **125** 180–204

[20] Bellouard Y 2008 Shape memory alloys for microsystems: a review from a material research perspective *Mater. Sci. Eng.* A **481–482** 582–9

[21] Liu K and Tovar A 2014 An efficient 3D topology optimization code written in Matlab *Struct. Multidiscip. Optim.* **50** 1175–96

[22] Zhu B, Zhang X, Zhang H, Liang J, Zang H, Li H and Wang R 2020 Design of compliant mechanisms using continuum topology optimization: a review *Mech. Mach. Theory* **143** 103622

[23] Sigmund O and Maute K 2013 Topology optimization approaches *Struct. Multidiscip. Optim.* **48** 1031–55

[24] Sigmund O 2011 On the usefulness of non-gradient approaches in topology optimization *Struct. Multidiscip. Optim.* **43** 589–96

[25] Bendsœ M P and Sigmund O 2011 *Topology Optimization: Theory, Methods and Applications (Engineering Online Library)* (Berlin: Springer)

[26] Alonso C, Ansola R and Querin O M 2014 Topology synthesis of multi-input–multi-output compliant mechanisms *Adv. Eng. Softw.* **76** 125–32

[27] Talischi C, Paulino G H, Pereira A and Menezes I F M 2012 PolyTop: a Matlab implementation of a general topology optimization framework using unstructured polygonal finite element meshes *Struct. Multidiscip. Optim.* **45** 329–57

[28] Sanogo S, Messine F, Hénaux C and Vilamot R 2014 Topology optimization for magnetic circuits dedicated to electric propulsion *IEEE Trans. Magn.* **50** 1–13

[29] Svanberg K 1987 The method of moving asymptotes—a new method for structural optimization *Int. J. Numer. Methods Eng.* **24** 359–73

[30] Taşkan E, Bulak S, Taşkan B, Şaşmaz M, El Abed S and El Abed A 2019 Nitinol as a suitable anode material for electricity generation in microbial fuel cells *Bioelectrochemistry* **128** 118–25

[31] Paik J K, Hawkes E and Wood R J 2010 A novel low-profile shape memory alloy torsional actuator *Smart Mater. Struct.* **19** 125014

[32] Paik J K and Wood R J 2012 A bidirectional shape memory alloy folding actuator *Smart Mater. Struct.* **21** 065013

[33] Liu X and Hua H 2013 On the characteristics of a quasi-zero stiffness isolator using Euler buckled beam as negative stiffness corrector *J. Sound Vib.* **332** 3359–76

[34] Velmurugan C, Senthilkumar V, Dinesh S and Arulkirubakaran D 2018 Machining of NiTi-shape memory alloys-a review *Mach. Sci. Technol.* **22** 355–401

[35] Nespoli A, Bettini P, Villa E, Sala G, Passaretti F and Grande A M 2021 A study on damping property of NiTi elements produced by selective laser-beam melting *Adv. Eng. Mater.* **23** 2001246

[36] Abdulhameed O, Al-Ahmari A, Ameen W and Mian S H 2019 Additive manufacturing: challenges, trends and applications *Adv. Mech. Eng.* **11** 1–27

[37] Tofail S A M, Koumoulos E P, Bandyopadhyay A, Bose S, O'Donoghue L and Charitidis C 2018 Additive manufacturing: scientific and technological challenges, market uptake and opportunities *Mater. Today* **21** 22–37

[38] Lee A Y, An J and Chua C K 2017 Two-way 4D printing: a review on the reversibility of 3D-printed shape memory materials *Engineering* **3** 663–74

[39] CSIRO 2020 World's first 3D printed NiTiNOL stent (available at: www.csiro.au/en/Research/MF/Areas/Metals/Lab22/3D-printed-Nitinol-stent) (accessed: November 2020)